Application of Total Least Squares to the Derivation of Closed-Form Green's Functions for Planar Layered Media

Rafael R. Boix, *Member, IEEE*, Francisco Mesa, *Member, IEEE*, and Francisco Medina, *Senior Member, IEEE*

Abstract—A new technique is presented for the numerical derivation of closed-form expressions of spatial-domain Green's functions for multilayered media. In the new technique, the spectral-domain Green's functions are approximated by an asymptotic term plus a ratio of two polynomials, the coefficients of these two polynomials being determined via the method of total least squares. The approximation makes it possible to obtain closed-form expressions of the spatial-domain Green's functions consisting of a term containing the near-field singularities plus a finite sum of Hankel functions. A judicious choice of the coefficients of the spectral-domain polynomials prevents the Hankel functions from introducing nonphysical singularities as the horizontal separation between source and field points goes to zero. The new numerical technique requires very few computational resources, and it has the merit of providing single closed-form approximations for the Green's functions that are accurate both in the near and far fields. A very good agreement has been found when comparing the results obtained with the new technique with those obtained via a numerically intensive computation of Sommerfeld integrals.

Index Terms—Green's functions, layered media, Sommerfeld integrals.

I. INTRODUCTION

THE application of the method of moments to the solution of mixed-potential integral equations has proven to be a powerful numerical tool in the analysis of planar circuits and antennas [1], [2], as well as in the study of the scattering properties of objects that are partially/completely buried in earth [3], [4]. In fact, current commercial software products that are extensively used in the design of planar circuits and antennas (such as Ansoft's Ensemble, Zeland's IE3D, and Agilent's Momentum) are based on a mixed-potential integral-equation approach. One crucial step in the application of the method of moments to mixed-potential integral equations is the numerical computation of spatial-domain Green's functions for the scalar and vector potentials in multilayered media [5], [6]. These Green's functions can be expressed as infinite integrals of spectral-domain

R. R. Boix and F. Medina are with the Microwaves Group, Department of Electronics and Electromagnetism, College of Physics, University of Seville, 41012 Seville, Spain (e-mail: boix@us.es).

F. Mesa is with the Microwaves Group, Department of Applied Physics 1, Escuela Técnica Superior de Ingeniería Informática, University of Seville, 41012 Seville, Spain (e-mail: mesa@us.es).

Green's functions that are commonly known as Sommerfeld integrals. Owing to the slowly decaying and highly oscillating behavior of the functions to be integrated, the brute-force numerical computation of Sommerfeld integrals is a time-consuming process. Therefore, in order to save CPU time in the solution of mixed-potential integral equations, an extensive research has been carried out over the last two decades to accelerate the computation of Sommerfeld integrals.

Some of the methods proposed for the fast computation of Sommerfeld integrals are based on tailor-made numerical integration techniques. These techniques include the weighted-average algorithm [5], [7] and related extrapolation algorithms [8], the integration along the imaginary axis of the spectral complex plane [7], [9], the integration along the steepest descent path [10], and the integration with a window function as a convolution kernel [11]. Although these techniques are all powerful numerical tools for the computation of Sommerfeld integrals, they have to be repeatedly used in the application of the method of moments as the distance between source and field points changes, which limits their numerical efficiency. One alternative, which partially alleviates this problem, is to combine numerical integration with the use of the fast Hankel transform [12]. A different approach to the computation of Sommerfeld integrals is based on the application of asymptotic methods such as the steepest descent method and the stationary phase method. These methods lead to asymptotic closed-form expressions of Green's functions that are valid in a wide range of distances between source and field points (typically above one wavelength) [10], [13], [14]. However, these expressions have been obtained only for simple layered media containing two or three different materials, and extension of the methods to layered media with an arbitrary number of materials seems to be a difficult task.

One method that has reached a prominent position in the computation of Green's functions for multilayered media is the discrete complex image method [15]–[31]. In this method, the spectral-domain Green's functions are approximated in terms of certain functions for which Sommerfeld integrals can be obtained in closed form. The method avoids numerical integration and provides results that are valid in a wide range of distances between source and field points. However, there is no common agreement in the functions that should be used in the approximation of the spectral-domain Green's functions. For some researchers, the spectral-domain Green's functions should be exclusively approximated in terms of complex exponentials that are fitted by means of the generalized pencil of functions or matrix pencil method [18], [19], [25], [26], [28], [30], [31]. One

drawback of this approach is that unpredictable large errors arise in the far-field computation of the spatial-domain Green's functions [27], [30]–[32]. Recently, Yuan *et al.* [31] have found that the value of ρ (horizontal separation between source and field points) marking the onset of far-field numerical errors can be made much larger by increasing the number of complex exponentials used in the approximations, but it may lead to a considerable CPU time consumption (see [31, Table I]). In accordance with the results shown in [27] and [29], the discrete complex image method improves its stability when the complex exponentials used in the approximations of the spectral Green's functions are accompanied by both a quasi-static term contributing the near field and a surface-waves term accounting for the far field. This is the approach originally proposed in [16] and followed in [17], [20]–[24], [27], and [29]. The drawback of this approach is that the surface-waves term contains poles of the spectral-domain Green's functions, as well as residues of the Green's functions at these poles, and the accurate determination of both the poles and the residues requires time-consuming algorithms [24], [29]. It has also been stated that the Hankel functions of the surface-waves term introduce near-field singularities in the spatial-domain Green's functions that do not exist when source and field points are placed in different horizontal planes of a multilayered media (i.e., when $z \neq z'$) [20], [23], [24]. Fortunately, this latter problem can be solved by using the error analysis technique proposed in [29].

A few years ago, Okhmatovski and Cangellaris introduced a new numerical method for the derivation of closed-form expressions for multilayered media Green's functions [32]. In their proposal, the spectral-domain Green's functions are represented in pole-residue form, and the poles and residues are numerically computed by means of a finite-difference approximation of the boundary value equations in the spectral domain. As a result of this, the spatial-domain Green's functions are expressed as finite series of Hankel functions representing cylindrical waves. The main drawback of this method is that the computational cost becomes very high in the near-field region since the number of terms required for the accurate approximation of the Green's functions grows very quickly as $\rho \to 0$. More recently, Cangellaris and his collaborators proposed an alternative formulation of the method where the poles and residues of the spectral-domain Green's functions are computed by means of an iterative algorithm called the vector-fitting algorithm [33], [34]. Although this new approach makes it possible to reduce the number of Hankel functions used in the approximation of the spatial-domain Green's functions, the vector-fitting algorithm is computationally demanding and does not suffice to eliminate the near-field numerical problems of the original method, as recognized in [34].

In this paper, a new numerical technique is presented for the derivation of closed-form Green's functions both in the spectral and spatial domains. The technique borrows several ideas from [32]–[34], but it does not share the drawbacks of the approaches followed in these papers. In the new technique, every spectral-domain Green's function is approximated in terms of an asymptotic term plus a fraction of two polynomials. The asymptotic terms are chosen in such a way that their spatial-domain counterparts account for the singular or quasi-singular be-

havior of the spatial-domain Green's functions as $\rho \to 0$ [34], [35]. Concerning the coefficients of the polynomials of the approximation, they are computed via the method of total least squares following an approach similar to that reported in [36]. Once an explicit expression for the fraction of polynomials is available, this expression is converted into a partial fraction expansion (pole-residue form), which makes it possible to write its spatial counterpart as a short series of Hankel functions. These Hankel functions introduce nonexisting singularities as $\rho \to 0$, but these singularities are eliminated by suppressing some of the polynomials coefficients. As a result, our technique leads to single closed-form expressions of the spatial Green's functions that are accurate both in the near and far fields (i.e., in the whole range of values of ρ), as it happens with the expressions of [29]. However, the CPU time required by the new technique is much smaller than that required in [29] for the following two main reasons.

- Although a singular-value decomposition is carried out by both the method of total least squares in the new technique and the matrix pencil method in the discrete complex image technique, the size of the matrix required by total least squares in the new technique is much smaller than that handled by the matrix pencil method in the discrete complex image technique, which considerably reduces the number of operations.
- The new technique only requires to compute the poles and residues of a fraction of polynomials, which is much simpler than computing the poles and residues of the spectral-domain Green's functions of an arbitrary multilayered media [29].

This paper is organized as follows. The derivation of closed-form expressions of multilayered media Green's functions is presented in Section II, which also describes in detail the strategies followed for eliminating nonexisting singularities both in the spectral- and spatial-domain approximations. Section III provides numerical results for the spatial-domain Green's functions of scalar and vector potentials both in the near and far fields. These results are compared with results obtained via numerical computation of Sommerfeld integrals, and good agreement is found in all cases. Conclusions are summarized in Section IV.

II. THEORY

Let (x, y, z) be the coordinates of an arbitrary field point in a multilayered substrate, and let (x', y', z') be the coordinates of an infinitesimal electric dipole source embedded in the multilayered substrate (since the treatment of magnetic sources is analogous to that of electric sources by virtue of the duality principle [6], only electric sources will be considered in this study). With respect to a reference frame centered at the source point, the radial and angular cylindrical coordinates of the field point will be (see [6, eq. (36)])

$$\rho = \sqrt{(x - x')^2 + (y - y')^2} \qquad (1)$$

$$\phi = \arctan\left(\frac{y - y'}{x - x'}\right). \qquad (2)$$

Among the different mixed-potential integral-equation formulations [6], it will be the formulation C of Michalski and Zheng [37] what will be used in this study. For the aforementioned electric source in a multilayered substrate, let $G_0(\rho)$ be a generic function representing either the corrected scalar potential Green's function K_ϕ of [37] or any of the diagonal elements of the corrected dyadic vector-potential Green's function $\overline{\mathbf{K}}_A$ of [37] ($\overline{\mathbf{K}}_A$ is defined in terms of the traditional vector-potential Green's function $\overline{\mathbf{G}}_A$ and the so-called *correction factor* $\mathbf{P} = P_z\hat{\mathbf{z}}$). In the frame of formulation C, the functions $G_0(\rho)$ can be written as Sommerfeld integrals of the type [37]

$$G_0(\rho) = S_0\{\widetilde{G}_0(k_\rho)\} = \frac{1}{2\pi}\int_{0(\text{SIP})}^{\infty} J_0(k_\rho\rho)\widetilde{G}_0(k_\rho)k_\rho dk_\rho \tag{3}$$

where $\widetilde{G}_0(k_\rho)$ is the spectral-domain counterpart of $G_0(\rho)$, $J_0(\cdot)$ is the Bessel function of first kind and order zero, and SIP is an integration path in the first quadrant of the complex k_ρ-plane that detours around the poles and branch points of $\widetilde{G}_0(k_\rho)$ (see [8, Fig. 1]).

Let $K_1(\rho, \phi)$ be a generic function representing any of the off-diagonal elements of $\overline{\mathbf{K}}_A$. In formulation C, the functions $K_1(\rho, \phi)$ can be all expressed in terms of Sommerfeld integrals of the type [37]

$$\begin{aligned} K_1(\rho, \phi) &= \begin{Bmatrix} \cos\phi \\ \sin\phi \end{Bmatrix} G_1(\rho) \\ &= \begin{Bmatrix} \cos\phi \\ \sin\phi \end{Bmatrix} S_1\{\widetilde{G}_1(k_\rho)\} \\ &= \begin{Bmatrix} \cos\phi \\ \sin\phi \end{Bmatrix} \left(\frac{1}{2\pi}\int_{0(\text{SIP})}^{\infty} J_1(k_\rho\rho)\widetilde{G}_1(k_\rho)k_\rho^2 dk_\rho\right) \end{aligned} \tag{4}$$

where $\widetilde{G}_1(k_\rho)$ is the spectral-domain counterpart of $G_1(\rho)$, $\cos\phi$ or $\sin\phi$ are multiplying factors ($\cos\phi$ appears in K_{xz}^A and K_{zx}^A, and $\sin\phi$ appears in K_{xy}^A and K_{yx}^A), and $J_1(\cdot)$ is the Bessel function of first kind and order 1.

In [32], Okhmatovski and Cangellaris used a finite-difference scheme to prove that the spectral-domain functions $\widetilde{G}_0(k_\rho)$ and $\widetilde{G}_1(k_\rho)$ can be approximately written as pole-residue finite series of the form

$$\widetilde{G}_n(k_\rho) \approx \sum_{i=1}^{M} \frac{a_{n,i}}{k_\rho^2 - (p_{n,i})^2}, \qquad n = 0, 1. \tag{5}$$

When (5) is introduced in (3) and (4), closed-form expressions of $G_0(\rho)$ and $G_1(\rho)$ are obtained in terms of finite sums of Hankel functions [32]. The problem with these finite sums is that they require a very large value of M for obtaining accurate values of $G_0(\rho)$ and $G_1(\rho)$ as $\rho \to 0$ [32]. In an attempt to overcome this problem, Kourkoulos and Cangellaris have recently suggested that the Hankel functions series should be combined with a closed-form quasi-static term accounting for the near-field contributions to the Green's functions [34]. Unfortunately, the introduction of this quasi-static term does not always suffice to solve the near-field convergence problems reported in [32]. The origin of these numerical problems is that the Hankel

functions used in [32] and [34] introduce nonphysical singularities as $\rho \to 0$, which is a well-known phenomenon [20], [23], [24], [29], [34]. If a quasi-static term is added to the Hankel functions, as in [34], the near-field problems are only eliminated in the particular cases where the Green's functions are singular as $\rho \to 0$ (e.g., $G_0(\rho)$ shows this behavior when the source and field points are in the same horizontal plane, i.e., when $z = z'$) since, in those cases, the quasi-static term is also singular, and this singularity dominates over the Hankel functions singularities [29]. However, when the Green's functions are not singular as $\rho \to 0$ (e.g., when the source and field points are in different horizontal planes, i.e., when $z \neq z'$), the quasi-static term is not singular either and, therefore, it cannot mask the nonphysical singularities introduced by the Hankel functions.

In the following, a new approach is proposed for calculating closed-form spatial-domain Green's functions. Our proposal is similar to that of [34], but does not suffer from inaccuracies related to Hankel functions singularities. In the new approach, the spectral-domain Green's functions $\widetilde{G}_0(k_\rho)$ and $\widetilde{G}_1(k_\rho)$ are written as

$$\widetilde{G}_n(k_\rho) \approx \widetilde{G}_n^{\text{as}}(k_\rho) + \sum_{i=1}^{M} \frac{a_{n,i}}{k_\rho^2 - p_{n,i}^2}, \qquad n = 0, 1 \tag{6}$$

where $\widetilde{G}_n^{\text{as}}(k_\rho)$ $(n = 0, 1)$ denotes the asymptotic behaviors of $\widetilde{G}_n(k_\rho)$ $(n = 0, 1)$ for large values of k_ρ. Note that, in (6), every spectral-domain Green's function is approximated by means of the pole-residue representation of (5) plus one asymptotic term. In accordance with the explanations of [38], the asymptotic terms $\widetilde{G}_0^{\text{as}}(k_\rho)$ and $\widetilde{G}_1^{\text{as}}(k_\rho)$ determine the behavior of $G_0(\rho)$ and $G_1(\rho)$ in the vicinity of $\rho = 0$, respectively. If (6) is to provide an accurate closed-form representation of the spatial-domain Green's functions, the asymptotic terms $\widetilde{G}_n^{\text{as}}(k_\rho)$ $(n = 0, 1)$ have to satisfy the following conditions.

- They must have closed-form inverse Hankel transforms, i.e., the Sommerfeld integrals arising from the introduction of $\widetilde{G}_n^{\text{as}}(k_\rho)$ $(n = 0, 1)$ in (3) and (4) must have closed-form expressions.
- Their spatial-domain counterpart should reproduce the singular or quasi-singular behavior of $G_0(\rho)$ and $G_1(\rho)$ as $\rho \to 0$.
- They should not have spectral-domain singularities different from those of $\widetilde{G}_0(k_\rho)$ and $\widetilde{G}_1(k_\rho)$.

The asymptotic expressions defined in [34] and [35] for the spectral-domain Green's functions of a source in a multilayered substrate are good candidates for $\widetilde{G}_n^{\text{as}}(k_\rho)$ $(n = 0, 1)$ since they fulfill the first two conditions (they have a closed-form inverse Hankel transform and they account for spatial-domain near-field singularities). However, they do not satisfy the third condition. In fact, the spectral asymptotic expressions proposed in [34] and [35] have "additional" singularities (either at $k_\rho = 0$ or at $k_\rho = k_0\sqrt{\epsilon_s\mu_s}$, where k_0 is the free-space wavenumber and ϵ_s and μ_s are the relative permittivity and permeability of the source layer) that are not present in $\widetilde{G}_0(k_\rho)$ and $\widetilde{G}_1(k_\rho)$. Thus, the direct use of the spectral asymptotic expressions of [34] and [35] in (6) would raise numerical inaccuracies. Demuynck *et al.* addressed a possible solution to the problem of singularities in the spectral asymptotic expressions. Their solution consists of

multiplying these expressions by a factor that cancels out the "additional" singularities and, at the same time, keeps the same asymptotic behavior for large k_ρ [38]. In this paper, we have applied the cancellation technique of [38] to the asymptotic expressions of [35], and the new resulting asymptotic expressions have been adopted for playing the role of $\widetilde{G}_n^{\mathrm{as}}(k_\rho)$ $(n = 0, 1)$ in (6). These new asymptotic expressions are no longer singular and satisfy the aforementioned three conditions. In Appendix I, the expressions of $\widetilde{G}_n^{\mathrm{as}}(k_\rho)$ $(n = 0, 1)$ are presented in the particular case of the spectral-domain Green's functions for a simple one-layer microstrip structure.

Once the asymptotic terms $\widetilde{G}_n^{\mathrm{as}}(k_\rho)$ $(n = 0, 1)$ of (6) have been chosen, the coefficients $a_{n,i}$ and $p_{n,i}$ $(n = 0, 1; i = 1, \ldots, M)$ have to be obtained. In [32], these coefficients are computed by means of a quasi-analytical method resulting from a finite-difference scheme. However, Kourkoulos and Cangellaris [34] employ an iterative numerical algorithm (the vector-fitting algorithm) based on pole relocation of complex starting poles [39]. In this paper, the approach used for the computation of $a_{n,i}$ and $p_{n,i}$ is also numerical, and it is based on the method of total least squares. In order to apply this method, the pole-residue term of (6) must be written as a fraction of two polynomials [36] as follows:

$$\widetilde{G}_n(k_\rho) \approx \widetilde{G}_n^{\mathrm{as}}(k_\rho) + \frac{\widetilde{P}_n^{(M-1)}\left(k_\rho^2\right)}{\widetilde{Q}_n^{(M)}\left(k_\rho^2\right)}, \qquad n = 0, 1 \quad (7)$$

where $\widetilde{P}_n^{(M-1)}\left(k_\rho^2\right)$ and $\widetilde{Q}_n^{(M)}\left(k_\rho^2\right)$ are polynomials in the variable k_ρ^2 of degrees $M-1$ and M, respectively. These two polynomials can be written as

$$\widetilde{P}_n^{(M-1)}\left(k_\rho^2\right) = \sum_{i=0}^{M-1} c_{n,i} k_\rho^{2i}, \qquad n = 0, 1 \quad (8)$$

$$\widetilde{Q}_n^{(M)}\left(k_\rho^2\right) = k_\rho^{2M} + \sum_{i=0}^{M-1} d_{n,i} k_\rho^{2i}, \qquad n = 0, 1 \quad (9)$$

where $c_{n,i}$ and $d_{n,i}$ are unknown coefficients that are related to the coefficients $a_{n,i}$ and $p_{n,i}$ of (6). When (8) and (9) are introduced in (7), and the resulting expression is multiplied by $\widetilde{Q}_n^{(M)}\left(k_\rho^2\right)$, it is obtained after some rearrangements that

$$\left[\widetilde{G}_n(k_\rho) - \widetilde{G}_n^{\mathrm{as}}(k_\rho)\right] k_\rho^{2M}$$
$$\approx -\sum_{i=0}^{M-1} d_{n,i} \left[\widetilde{G}_n(k_\rho) - \widetilde{G}_n^{\mathrm{as}}(k_\rho)\right] k_\rho^{2i}$$
$$+ \sum_{i=0}^{M-1} c_{n,i} k_\rho^{2i}, \qquad n = 0, 1. \quad (10)$$

Each of the equations of (10) poses one problem of linear parameter estimation with unknown parameters $c_{n,i}$ and $d_{n,i}$, and for each of these problems, there is a best solution in the total least squares sense. In order to obtain that solution, the approximate expression of (10) is enforced to be exactly satisfied at $N > 2M$ different values of the complex variable k_ρ, $k_\rho = k_{\rho i}$ $(i = 1, \ldots, N)$, which yields an overdetermined system of linear equations. As explained in [40], this linear system of
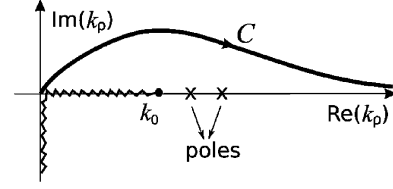

Fig. 1. Path chosen in the complex k_ρ / k_0-plane when applying the method of total least squares to (10).

equations can be solved via a singular-value decomposition for obtaining the minimum total least squares solution. Since the spectral-domain Green's functions of lossless multilayered substrates have surface-wave singularities and branch-point singularities along the real axis of the complex k_ρ-plane [5], in the application of the method of total least squares, it is convenient to sample (10) along a path in the complex k_ρ-plane that detours around the singularities [16]. In this study, we have chosen a path, i.e., C, that satisfies this last condition and that asymptotically approaches the real axis of the k_ρ-plane; specifically

$$C: \frac{k_\rho}{k_0} = t \left[1 + jAe^{(1-t)}\right] 0 \le t \le T_0 \quad (11)$$

where A determines the maximum imaginary value taken by the path. The path defined by (11) is shown in Fig. 1. In our experience, a good choice is to take $A = 0.1$ and $T_0 \approx 1.2 k_{\max}/k_0$ in (11), where $k_{\max}$ is the maximum wavenumber among the layers of the multilayered substrate. Anyway, numerical simulations have proven that the results obtained via the method of total least squares (see Section III) are not appreciably sensitive to slight variations in the aforementioned values of A and T_0.

Once a total least squares solution has been obtained for the coefficients $c_{n,i}$ and $d_{n,i}$ of (10), the coefficients $p_{n,i}^2$ of (6) (i.e., the squared poles of the pole-residue term) can be determined as the complex roots of the polynomial $\widetilde{Q}_n^{(M)}\left(k_\rho^2\right)$. These roots can be readily extracted from the polynomial coefficients by computing the eigenvalues of the companion matrix, as explained in [41]. The coefficients $a_{n,i}$ can also be obtained in terms of $p_{n,i}^2$ by using the standard residue definition

$$a_{n,i} = \lim_{k_\rho^2 \to p_{n,i}^2} \left(k_\rho^2 - p_{n,i}^2\right) \frac{\widetilde{P}_n^{(M-1)}\left(k_\rho^2\right)}{\widetilde{Q}_n^{(M)}\left(k_\rho^2\right)}$$
$$= \frac{\widetilde{P}_n^{(M-1)}\left(p_{n,i}^2\right)}{\left.\dfrac{dQ_n^{(M)}\left(k_\rho^2\right)}{dk_\rho^2}\right|_{k_\rho^2 = p_{n,i}^2}}, \qquad n = 0, 1. \quad (12)$$

Regarding the computation of the coefficients $a_{n,i}$ and $p_{n,i}^2$ of (6), the application of the method of total least squares has two advantages over the vector-fitting algorithm [34]. First, whereas the method of total least squares generates the poles and residues in one step, the vector-fitting algorithm carries out an iterative search, the computation time required by each iteration being comparable to that required by the method of total least squares as a whole. The second advantage is that the method of total least squares gives an estimate for M (the number of terms retained in the pole-residue series) from the number of nonzero

singular values obtained in the singular-value decomposition [36]. In Section III, it will be shown that values of M lower than 13 have always been found sufficient to obtain accurate approximations of $\widetilde{G}_n(k_\rho)$ ($n = 0, 1$). These values of M are certainly smaller than those handled in [33] and [34], and considerably smaller than those reported in [32].

When the approximation proposed in (6) is introduced in (3) and (4), and the Sommerfeld integrals are calculated [42], the following expressions are obtained:

$$S_0\{\widetilde{G}_0(k_\rho)\} \approx G_0^{\mathrm{as}}(\rho) - \frac{j}{4}\sum_{i=1}^{M} a_{0,i} H_0^{(2)}(p_{0,i}\rho) \tag{13}$$

$$S_1\{\widetilde{G}_1(k_\rho)\} \approx G_1^{\mathrm{as}}(\rho) - \frac{j}{4}\sum_{i=1}^{M} a_{1,i} p_{1,i} H_1^{(2)}(p_{1,i}\rho) \tag{14}$$

where $H_n^{(2)}(\cdot)$ ($n = 0, 1$) are Hankel functions of the second kind and order n, and $G_0^{\mathrm{as}}(\rho)$ and $G_1^{\mathrm{as}}(\rho)$ can be written in closed form in terms of functions of the type shown in (45) and (47). As mentioned above, the complex roots of the polynomial $\widetilde{Q}_n^{(M)}\left(k_\rho^2\right)$ provide the numerical values of $p_{n,i}^2$ ($n = 0, 1$; $i = 1, \ldots, M$). Since the complex numbers $+\sqrt{p_{n,i}^2}$ and $-\sqrt{p_{n,i}^2}$ ($n = 0, 1$; $i = 1, \ldots, M$) are all poles of $\widetilde{G}_n(k_\rho)$ [see (6)], the sign of the poles $p_{n,i}$ used in (13) and (14) has to be chosen in such a way that $-\pi < \arg\{p_{n,i}\} \le 0$, which ensures that the solution obtained for $G_0^{\mathrm{as}}(\rho)$ and $G_1^{\mathrm{as}}(\rho)$ fulfills the causality and radiation conditions [34].

As commented above, the functions $G_0^{\mathrm{as}}(\rho)$ and $G_1^{\mathrm{as}}(\rho)$ of (13) and (14) reproduce the behavior of $G_0(\rho)$ and $G_1(\rho)$ as $\rho \to 0$. In fact, $G_0^{\mathrm{as}}(\rho)$ and $G_1^{\mathrm{as}}(\rho)$ may have singularities as $\rho \to 0$, and these singularities coincide with those of $G_0(\rho)$ and $G_1(\rho)$ (as stated above, the singularities may be present when the source and field points are in the same horizontal plane $z = z'$, but they never appear when the source and field points are in different horizontal planes $z \ne z'$). The Hankel functions $H_0^{(2)}(p_{0,i}\rho)$ and $H_1^{(2)}(p_{1,i}\rho)$ of (13) and (14) also have singularities as $\rho \to 0$, but these singularities are not shared by $G_0(\rho)$ and $G_1(\rho)$, and this may have a detrimental effect on the accuracy of (13) and (14) as $\rho \to 0$ [20], [23], [24]. In the remainder of this section, it will be shown that the coefficients $a_{n,i}$ can be chosen in such a way that the sums of Hankel functions of (13) and (14) have a nonsingular smooth behavior in the vicinity of $\rho \to 0$. In that case, the series of Hankel functions will not mask the correct behavior of $G_0(\rho)$ and $G_1(\rho)$ as $\rho \to 0$, which is provided by $G_0^{\mathrm{as}}(\rho)$ and $G_1^{\mathrm{as}}(\rho)$.

In order to show the problem of Hankel functions singularities in the case of (13), the following expansion of $H_0^{(2)}(p_{0,i}\rho)$ as $\rho \to 0$ [43] is used:

$$\left. H_0^{(2)}(p_{0,i}\rho)\right|_{\rho \to 0}$$
$$= -\frac{2j}{\pi}\ln\rho + \left[1 - \frac{2j}{\pi}\left(\gamma + \ln\left(\frac{p_{0,i}}{2}\right)\right)\right]$$
$$+ \frac{j(p_{0,i})^2}{2\pi}\rho^2\ln\rho + O(\rho^2), \qquad i = 1, \ldots, M \tag{15}$$

where γ is Euler's constant [43]. If (15) is introduced in (13), the following expansion of $S_0\{\widetilde{G}_0(k_\rho)\}$ as $\rho \to 0$ is obtained:

$$\left. S_0\{\widetilde{G}_0(k_\rho)\}\right|_{\rho \to 0}$$
$$\approx \left. G_0^{\mathrm{as}}(\rho)\right|_{\rho \to 0} - \frac{1}{2\pi}\ln\rho\sum_{i=1}^{M} a_{0,i}$$
$$- \frac{j}{4}\left[1 - \frac{2j}{\pi}(\gamma - \ln 2)\right]\sum_{i=1}^{M} a_{0,i}$$
$$- \frac{1}{2\pi}\sum_{i=1}^{M} a_{0,i}\ln p_{0,i} + \frac{1}{8}\rho^2\ln\rho\sum_{i=1}^{M} a_{0,i}(p_{0,i})^2. \tag{16}$$

Equation (16) shows that the Hankel functions of (13) introduce a logarithmic singularity as $\rho \to 0$. However, note that this logarithmic singularity can be suppressed if $\sum_{i=1}^{M} a_{0,i} = 0$ is enforced. Looking at (6) and (7), the sum $\sum_{i=1}^{M} a_{0,i}$ can be related to the coefficients of the polynomial $\widetilde{P}_0^{(M-1)}\left(k_\rho^2\right)$ in the following way:

$$\sum_{i=1}^{M} a_{0,i} = \lim_{k_\rho \to \infty} k_\rho^2 \sum_{i=1}^{M}\frac{a_{0,i}}{k_\rho^2 - p_{0,i}^2}$$
$$= \lim_{k_\rho \to \infty} k_\rho^2 \frac{\widetilde{P}_0^{(M-1)}\left(k_\rho^2\right)}{\widetilde{Q}_0^{(M)}\left(k_\rho^2\right)} = c_{0,M-1}. \tag{17}$$

Therefore, if $\sum_{i=1}^{M} a_{0,i} = 0$ is enforced, the coefficient $c_{0,M-1}$ of $\widetilde{P}_0^{(M-1)}\left(k_\rho^2\right)$ must be set to zero. According to this result, in order to avoid the effect of Hankel functions singularities as $\rho \to 0$ in (13), a polynomial in k_ρ^2 of degree $M - 2$ should be used in the numerator of the approximation (7) of $\widetilde{G}_0(k_\rho)$. Thus, it is convenient to approximate $\widetilde{G}_0(k_\rho)$ as

$$\widetilde{G}_0(k_\rho) \approx \widetilde{G}_0^{\mathrm{as}}(k_\rho) + \frac{\widetilde{P}_0^{(M-2)}\left(k_\rho^2\right)}{\widetilde{Q}_0^{(M)}\left(k_\rho^2\right)} \tag{18}$$

where

$$\widetilde{P}_0^{(M-2)}\left(k_\rho^2\right) = \sum_{i=0}^{M-2} c_{0,i} k_\rho^{2i}. \tag{19}$$

The procedure designed for avoiding the effect of Hankel functions singularities in (13) can also be applied to (14). In this latter case, the analysis of the singularities suggests to use the following expansion of the functions $H_1^{(2)}(p_{1,i}\rho)$ as $\rho \to 0$ [43]:

$$\left. H_1^{(2)}(p_{1,i}\rho)\right|_{\rho \to 0}$$
$$= \frac{2j}{\pi p_{1,i}\rho} - \frac{jp_{1,i}\rho}{\pi}\ln\rho$$
$$+ \frac{p_{1,i}\rho}{2}\left[1 - \frac{2j}{\pi}\ln\left(\frac{p_{1,i}}{2}\right) + \frac{j}{\pi}(1 - 2\gamma)\right]$$
$$+ O(\rho^3\ln\rho), \qquad i = 1, \ldots, M. \tag{20}$$

Equation (20) must then be introduced in (14) in order to obtain the expansion of $S_1\{\widetilde{G}_1(k_\rho)\}$ as $\rho \to 0$

$$
\begin{aligned}
S_1\{\widetilde{G}_1(k_\rho)\}\Big|_{\rho \to 0} \\
\approx G_1^{\text{as}}(\rho)\Big|_{\rho \to 0} + \frac{1}{2\pi\rho} \sum_{i=1}^{M} a_{1,i} \\
- \frac{1}{4\pi} \rho \ln\rho \sum_{i=1}^{M} a_{1,i}(p_{1,i})^2 \\
- \frac{j\rho}{8}\left[1 + \frac{2j}{\pi}\ln 2 + \frac{j}{\pi}(1-2\gamma)\right]\sum_{i=1}^{M} a_{1,i}(p_{1,i})^2 \\
- \frac{\rho}{4\pi}\sum_{i=1}^{M} a_{1,i}(p_{1,i})^2 \ln p_{1,i}.
\end{aligned} \tag{21}
$$

Equation (21) shows that the Hankel functions of (14) introduce a singularity of the type ρ^{-1} as $\rho \to 0$. This singularity can be eliminated provided that $\sum_{i=1}^{M} a_{1,i} = 0$ is enforced. However, this condition does not always suffice to ensure that the Hankel functions of (14) do not mask the behavior of $G_1^{\text{as}}(\rho)$ as $\rho \to 0$. In fact, since $G_1^{\text{as}}(\rho) \propto \rho$ as $\rho \to 0$ and $z \neq z'$ (see [21, eq. (24)]) and $\sum_{i=1}^{M} a_{1,i}p_{1,i}H_1^{(2)}(p_{1,i}\rho) \propto \rho\ln\rho$ as $\rho \to 0$ and $\sum_{i=1}^{M} a_{1,i} = 0$, $G_1^{\text{as}}(\rho)$ may tend to zero faster than $\sum_{i=1}^{M} a_{1,i}p_{1,i}H_1^{(2)}(p_{1,i}\rho)$ as $\rho \to 0$. If $\sum_{i=1}^{M} a_{1,i}p_{1,i}H_1^{(2)}(p_{1,i}\rho)$ has to go to zero faster than $G_1^{\text{as}}(\rho)$ (or at least with the same decay rate), it is then necessary that not only $\sum_{i=1}^{M} a_{1,i} = 0$ in (21), but also $\sum_{i=1}^{M} a_{1,i}(p_{1,i})^2 = 0$. The two finite sums $\sum_{i=1}^{M} a_{1,i}$ and $\sum_{i=1}^{M} a_{1,i}(p_{1,i})^2$ can be related to the coefficients of the polynomial $\widetilde{P}_1^{(M-1)}(k_\rho^2)$ in the following way:

$$
\begin{aligned}
\sum_{i=1}^{M} a_{1,i} &= \lim_{k_\rho \to \infty} k_\rho^2 \sum_{i=1}^{M} \frac{a_{1,i}}{k_\rho^2 - p_{1,i}^2} \\
&= \lim_{k_\rho \to \infty} k_\rho^2 \frac{\widetilde{P}_1^{(M-1)}(k_\rho^2)}{\widetilde{Q}_1^{(M)}(k_\rho^2)} = c_{1,M-1}
\end{aligned} \tag{22}
$$

$$
\begin{aligned}
\sum_{i=1}^{M} a_{1,i}(p_{1,i})^2 &= \lim_{k_\rho \to \infty} k_\rho^4\left[\sum_{i=1}^{M} \frac{a_{1,i}}{k_\rho^2 - p_{1,i}^2} - \frac{\sum_{i=1}^{M} a_{1,i}}{k_\rho^2}\right] \\
&= \lim_{k_\rho \to \infty} k_\rho^4\left[\frac{\widetilde{P}_1^{(M-1)}(k_\rho^2)}{\widetilde{Q}_1^{(M)}(k_\rho^2)} - \frac{c_{1,M-1}}{k_\rho^2}\right] \\
&= c_{1,M-2}.
\end{aligned} \tag{23}
$$

Therefore, if $\sum_{i=1}^{M} a_{1,i} = 0$ and $\sum_{i=1}^{M} a_{1,i}(p_{1,i})^2 = 0$ are both enforced, the coefficients $c_{1,M-1}$ and $c_{1,M-2}$ of $\widetilde{P}_1^{(M-1)}(k_\rho^2)$ must be set to zero. In conclusion, in order to avoid the effect of Hankel functions singularities in the approximation (14) of $S_1\{\widetilde{G}_1(k_\rho)\}$ as $\rho \to 0$, the polynomial of the numerator in the approximation (7) of $\widetilde{G}_1(k_\rho)$ has to be a polynomial in k_ρ^2 of
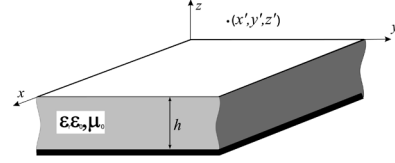

Fig. 2. One-layer substrate microstrip structure studied in this paper. The source point is in the air.

degree $M - 3$. Thus, the approximation of $\widetilde{G}_1(k_\rho)$ should be written as

$$
\widetilde{G}_1(k_\rho) \approx \widetilde{G}_1^{\text{as}}(k_\rho) + \frac{\widetilde{P}_1^{(M-3)}(k_\rho^2)}{\widetilde{Q}_1^{(M)}(k_\rho^2)} \tag{24}
$$

where

$$
\widetilde{P}_1^{(M-3)}(k_\rho^2) = \sum_{i=0}^{M-3} c_{1,i}k_\rho^{2i}. \tag{25}
$$

It should be noted that the pole-residue terms of (6) and (7) were originally proposed to decay at a rate k_ρ^{-2} for large k_ρ. However, in order to avoid problems in the approximation of the spatial-domain Green's functions as $\rho \to 0$, it has now been proven that the pole-residue term of $\widetilde{G}_0(k_\rho)$ should decay at a rate k_ρ^{-4} for large k_ρ, and the pole-residue term of $\widetilde{G}_1(k_\rho)$ at a rate k_ρ^{-6}. This conclusion can be connected with the error analysis carried out in [29] where it was shown that singularity problems encountered for $\rho \to 0$ in the application of the discrete complex image method can be solved when the surface-wave term of $\widetilde{G}_0(k_\rho)$ decays at a rate k_ρ^{-4} for large k_ρ, and the surface-wave term of $\widetilde{G}_1(k_\rho)$ decays at a rate k_ρ^{-8}. Whereas the former result is coherent with that obtained in this paper, there is a discrepancy in the latter result. In our opinion, the decay rate imposed in [29] to the surface-wave term of $\widetilde{G}_1(k_\rho)$ may be stricter than necessary. In fact, if that surface-wave term is enforced to decay at a rate k_ρ^{-6}, this may probably suffice to eliminate the singularity problems discussed in [29].

III. NUMERICAL RESULTS

For demonstrative purposes, the method of Section II has been applied to the computation of the Green's functions of the simple microstrip structure of Fig. 2 when the value of the relative permittivity is $\epsilon_r = 4.4$ and the value of the substrate thickness is $h = 10$ mm. The results are presented in Figs. 3–11.

Fig. 3 shows results for the spectral-domain scalar potential Green's function along the path of Fig. 1. An excellent agreement is found when the exact values of the spectral-domain Green's function are compared with the values arising from the application of the method of total least squares (18) (in all the figures in this section, the results obtained via the method of total least squares will be denoted as TLS). The differences between the two sets of results are always found to be below 0.03%. Since the approximation provided by the spectral-domain expression (18) is very accurate, the approximation provided by its spatial-domain counterpart (13) should also be very accurate. This is verified in Fig. 4 where the results obtained with the closed-form expression (13) are compared with results obtained via numerical integration of Sommerfeld integrals. Again, the
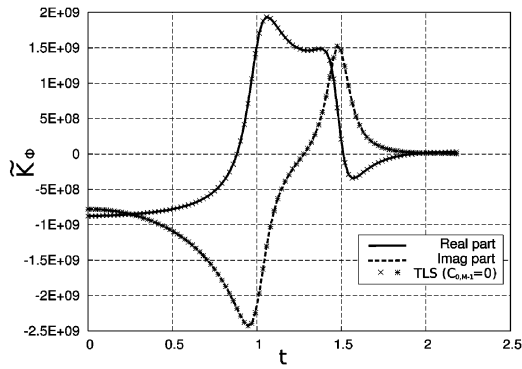
Fig. 3. Real and imaginary parts of spectral-domain Green's function $\widetilde{K}_\phi$ along path C of Fig. 1. The exact results (solid and dashed line) are compared with those obtained via the method of TLS following (18) ($\times$, $*$). $f = 4.075$ GHz, $z' = z = 0$, $A = 0.1$, $T_0 = 2.2$, $M = 12$, $N = 27$.
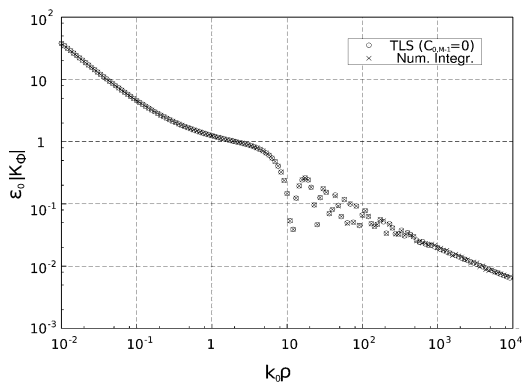

Fig. 4. Magnitude of the spatial-domain Green's function K_ϕ. Numerical integration results ($\times$) are compared with those obtained via (13) when $c_{0,M-1} = 0$ ($\circ$). $f = 4.075$ GHz, $z = z' = 0$, $A = 0.1$, $T_0 = 2.2$, $M = 12$, $N = 27$.
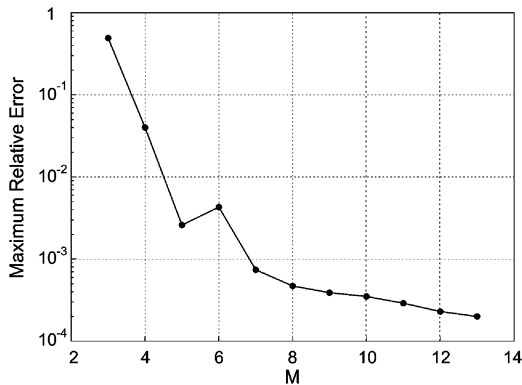

Fig. 5. Magnitude of the maximum relative error detected along path C of (11) in the total least squares approximation of $\widetilde{K}_\phi$ in Fig. 3. The maximum relative error is plotted versus the number of pole-residue terms retained in (6) ($A = 0.1$, $T_0 = 2.2$, $N = 2M + 3$).

Fig. 6. Real and imaginary parts of spectral-domain Green's function $\widetilde{K}_{xx}^A$ along path C of Fig. 1. The exact results (solid and dashed lines) are compared with those obtained via (18) ($\times$, $*$). $f = 25$ GHz, $z' = 0.5$ mm, $z = -0.5$ mm, $A = 0.1$, $T_0 = 2.5$, $M = 12$, $N = 27$.

Fig. 7. Magnitude of the spatial-domain Green's function K_{xx}^A. Numerical integration results ($\times$) are compared with those obtained via (13) when $c_{0,M-1} = 0$ ($\circ$). $f = 25$ GHz, $z' = 0.5$ mm, $z = -0.5$ mm, $A = 0.1$, $T_0 = 2.5$, $M = 12$, $N = 27$.

Fig. 8. Magnitude of the spatial-domain Green's function K_{xx}^A. The results obtained via (13) when $c_{0,M-1} = 0$ ($\circ$) are compared with those obtained via (13) when $c_{0,M-1} \neq 0$ ($\times$). $f = 25$ GHz, $z' = 0.5$ mm, $z = -0.5$ mm, $A = 0.1$, $T_0 = 2.5$, $M = 12$, $N = 27$.

agreement between the two sets of results is excellent for both small and large values of ρ. The structure studied in Figs. 3 and 4 has already been analyzed in [9, Fig. 6(a)]. This structure was claimed to be troublesome because the spectral-domain Green's function has a pole in the real axis of the complex k_ρ-plane that is very close to the branch point at $k_\rho = k_0$. According to [9], this has an influence on the terms contributing the far-field behavior of the spatial-domain Green's function. Fortunately, Figs. 3 and 4 clearly show that the aforementioned problem does
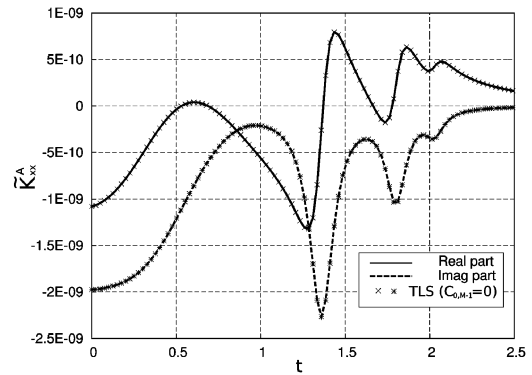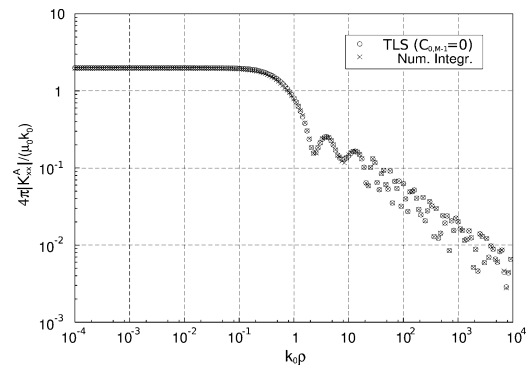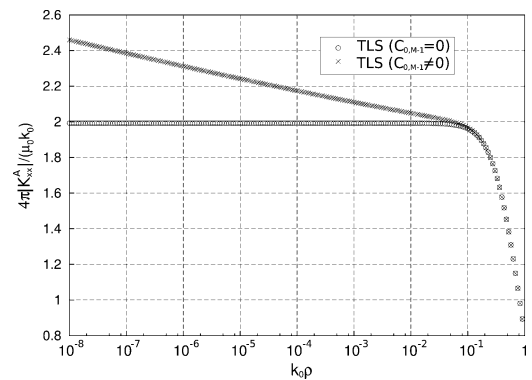
not affect the approximations provided by (13) and (18). Fig. 4 shows that only 12 Hankel functions are needed in (13) for obtaining accurate values of the spatial-domain Green's function along six decades of the variable $k_0\rho$, and this number of Hankel functions is roughly half of that handled in [34] for a similar accuracy, and one order of magnitude smaller than that handled in [32]. The computation of the total least squares results plotted in Fig. 4 also requires the singular-value decomposition of a
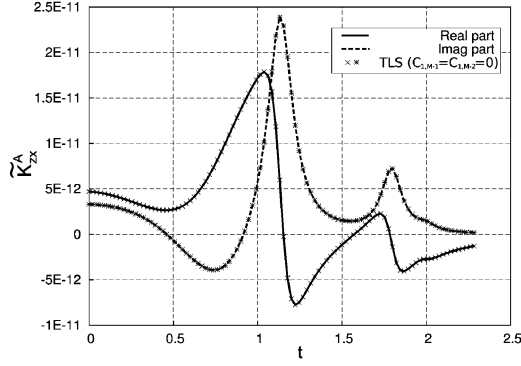
Fig. 9. Real and imaginary parts of spectral-domain Green's function $\widetilde{K}_{zx}^{A}$ along path C of Fig. 1. The exact results (solid and dashed line) are compared with those obtained via (24) ($\times, *$). $f = 11$ GHz, $z' = 1$ mm, $z = 0$ mm, $A = 0.1$, $T_0 = 2.3$, $M = 13$, $N = 29$.
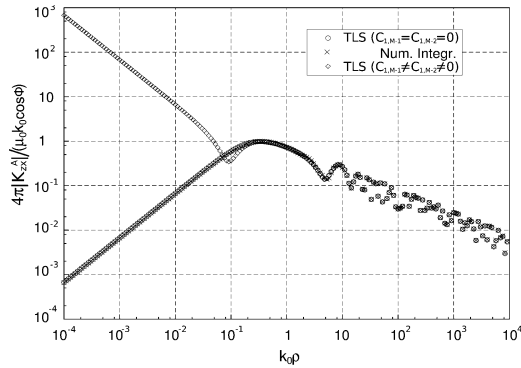

Fig. 10. Magnitude of the spatial-domain Green's function K_{zx}^{A}. Numerical integration results ($\times$) are compared with those obtained via (14) when $c_{1,M-1} = c_{1,M-2} = 0$ ($\circ$), and with those obtained via (14) when $c_{1,M-1} \neq 0$ and $c_{1,M-2} \neq 0$ ($\diamond$). $f = 11$ GHz, $z' = 1$ mm, $z = 0$ mm, $A = 0.1$, $T_0 = 2.3$, $M = 13$, $N = 29$.
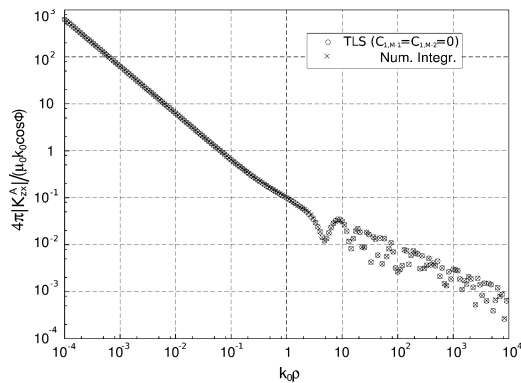

Fig. 11. Magnitude of the spatial-domain Green's function K_{zx}^{A}. Numerical integration results ($\times$) are compared with those obtained via (14) when $c_{1,M-1} = c_{1,M-2} = 0$ ($\circ$). $f = 11$ GHz, $z' = z = 0$ mm, $A = 0.1$, $T_0 = 2.3$, $M = 13$, $N = 29$.

24×27 matrix. According to [32, Sec. V], this singular-value decomposition needs a computation time that is considerably smaller than that needed by the singular-value decomposition of the matrices usually involved in the application of both the discrete complex image method and the method of [32].

In Fig. 5, the maximum relative error made in the TLS approximation of the spectral Green's function $\widetilde{K}_{\phi}$ of Fig. 3 is plotted as a function of M [M denotes the number of pole-residue terms used in (6)]. This maximum relative error is obtained by computing the relative error between the exact and approximate values of $\widetilde{K}_{\phi}$ along 200 points of the path C of Fig. 1. The results of Fig. 5 show that the accuracy of the approximation obtained via (18) increases as M increases, and the maximum relative error remains below 0.1% for $M \geq 7$. Values of $M \geq 14$ are not shown because there appear zero singular values in the corresponding singular-value decompositions. It has then been checked that the method of total least squares has a robust convergence pattern concerning the number of pole-residue terms included in the approximation of the spectral-domain Green's functions.

Fig. 6 shows the xx component of the spectral-domain vector-potential Green's function along the path C of Fig. 1. The exact values of $\widetilde{K}_{xx}^{A}$ are compared with the values provided by (18), and excellent agreement is found (relative errors less than 0.1%). At the operating frequency $f = 25$ GHz, the spectral-domain Green's function $\widetilde{K}_{xx}^{A}$ presents three TE poles on the real axis of the complex k_{ρ}-plane [7]. The three poles can be identified as peaks of the real and imaginary parts of $\widetilde{K}_{xx}^{A}$ in Fig. 6. Fig. 7 shows the spatial-domain counterpart of the spectral-domain Green's function $\widetilde{K}_{xx}^{A}$ approximated via (18). This spatial-domain counterpart is compared with the values of K_{xx}^{A} obtained via numerical integration of Sommerfeld integrals, and good agreement is found along eight decades of the variable $k_{0}\rho$. Note that the spatial-domain Green's function K_{ϕ} plotted in Fig. 4 has a singularity of the type ρ^{-1} as $\rho \rightarrow 0$ (in that case, the source and field points are in the same horizontal plane), but the spatial-domain Green's function K_{xx}^{A} of Fig. 7 is not singular as $\rho \rightarrow 0$ (the source and field points are now in different horizontal planes). As commented upon in Section II, in order to obtain an accurate approximation of K_{xx}^{A} via (13) for the case treated in Fig. 7, it is crucial to remove the logarithmic singularity of the Hankel functions as $\rho \rightarrow 0$. Fig. 8 shows the results obtained for K_{xx}^{A} via the method of Section II when the Hankel functions singularity is removed ($c_{0,M-1} = 0$), and when it is not removed ($c_{0,M-1} \neq 0$). As shown in Fig. 7, the results obtained when $c_{0,M-1} = 0$ match those obtained from numerical integration and, therefore, they can be assumed to be virtually correct. However, the results obtained when $c_{0,M-1} \neq 0$ in Fig. 8 are not correct because they deviate from those obtained when $c_{0,M-1} = 0$ for $k_{0}\rho < 10^{-1}$. In fact, the smaller the value of $k_{0}\rho$, the larger the deviation is. Fig. 8 shows that the curve obtained for the case $c_{0,M-1} \neq 0$ becomes a straight line with negative slope for $k_{0}\rho < 10^{-1}$. Since the vertical scale in Fig. 8 is linear and the horizontal scale is logarithmic, this fact points out that the approximation obtained for K_{xx}^{A} in the case $c_{0,M-1} \neq 0$ has a logarithmic singularity [which has not been removed from the Hankel functions of (13)]. This logarithmic singularity is not present in K_{xx}^{A}, and justifies why the approximation obtained for K_{xx}^{A} in the case $c_{0,M-1} \neq 0$ is not correct.

Whereas Fig. 8 illustrates how the technique of Section II provides accurate closed-form expressions of the spatial-domain Green's functions for small ρ, Table I(A) and (B) is introduced

TABLE I

NORMALIZED POLES AND RESIDUES OF THE SPECTRAL-DOMAIN GREEN'S FUNCTION $\widetilde{K}_{xx}^{A}(k_\rho)$ STUDIED IN FIG. 6.
(A) RESULTS OBTAINED BY USING THE APPROXIMATED EXPRESSION OF (18). (B) RESULTS OBTAINED
BY USING THE EXACT EXPRESSION VIA A NUMERICAL ALGORITHM

(A) Method of total least squares		
i	$p_{0,i}/k_0$	$a_{0,i} = R_{0,i}/2p_{0,i}$
1	$3.417501 \times 10^{-1} - j2.790234$	$-1.531848 \times 10^{-9} - j1.344238 \times 10^{-10}$
2	$4.856260 \times 10^{-1} - j4.100791 \times 10^{-1}$	$1.022622 \times 10^{-9} + j1.463123 \times 10^{-10}$
3	$-6.780465 \times 10^{-1} - j5.042418$	$5.918429 \times 10^{-10} + j3.051008 \times 10^{-10}$
4	$3.997048 \times 10^{-1} - j1.006589$	$-6.099622 \times 10^{-10} - j2.292849 \times 10^{-10}$
5	$\mathbf{1.358192 + j2.479521 \times 10^{-9}}$	$\mathbf{5.138023 \times 10^{-10} - j1.470549 \times 10^{-15}}$
6	$7.823941 \times 10^{-1} - j4.260563 \times 10^{-1}$	$-2.877646 \times 10^{-10} - j6.751015 \times 10^{-11}$
7	$\mathbf{1.798364 - j1.179428 \times 10^{-9}}$	$\mathbf{2.534032 \times 10^{-10} - j4.263823 \times 10^{-17}}$
8	$\mathbf{2.026230 - j4.124476 \times 10^{-9}}$	$\mathbf{6.535764 \times 10^{-11} + j2.987904 \times 10^{-19}}$
9	$9.357370 \times 10^{-1} - j1.677729 \times 10^{-1}$	$-1.697139 \times 10^{-11} - j1.414403 \times 10^{-11}$
10	$1.039687 \times 10^{-1} - j2.155948 \times 10^{-1}$	$-2.334194 \times 10^{-13} - j4.155695 \times 10^{-12}$
11	$9.859850 \times 10^{-1} - j3.515123 \times 10^{-2}$	$-1.914477 \times 10^{-13} - j1.792739 \times 10^{-12}$
12	$1.942305 \times 10^{-2} - j5.385078 \times 10^{-2}$	$-5.661670 \times 10^{-14} - j1.002621 \times 10^{-13}$

(B) Numerical algorithm		
i	$p_{0,i}^{\mathrm{num}}/k_0$	$R_{0,i}^{\mathrm{num}}/2p_{0,i}^{\mathrm{num}}$
1	**1.358179**	$\mathbf{5.138171 \times 10^{-10}}$
2	**1.798359**	$\mathbf{2.533952 \times 10^{-10}}$
3	$\mathbf{2.026229 - j1.692337 \times 10^{-8}}$	$\mathbf{6.535374 \times 10^{-11} - j6.156136 \times 10^{-17}}$

to explain why these closed-form expressions are accurate for large ρ. Table I(A) and (B) is similar to [34, Table I]. Table I(A) shows the normalized poles and the normalized residues of the approximate expression of $\widetilde{K}_{xx}^A$ obtained via (18) for the structure of Figs. 6–8 (in accordance with (6), the residue of this approximate expression of $\widetilde{K}_{xx}^A$ at the pole $p_{0,i}$ will be given by $R_{0,i} = 2a_{0,i}p_{0,i}$). The sign of these poles and residues has been chosen so that they can be used in the finite series of Hankel functions of (13). Since $H_0^{(2)}(p_{0,i}\rho) \propto e^{-jp_{0,i}\rho}/\sqrt{p_{0,i}\rho}$ for large ρ, the Hankel functions of (13) involving poles $p_{0,i}$ with large negative imaginary part will be negligible for large ρ, and those Hankel functions involving poles $p_{0,i}$ with very small imaginary part will not be negligible. In Table I(A), the imaginary part of poles 5, 7, and 8 are at least seven orders of magnitude smaller than the remaining ones. Therefore, the Hankel functions involving these three poles will prevail over the rest of Hankel functions of (13) for large ρ. The three Hankel functions will also prevail over the function $G_0^{\mathrm{as}}(\rho)$ of (13) for large ρ [the behavior of these Hankel functions is of the type $\rho^{-1/2}$, whereas that of $G_0^{\mathrm{as}}(\rho)$ is of the type ρ^{-3}, as can be demonstrated from (45)]. Thus, the approximate expression given by (13) for the Green's function K_{xx}^A of Fig. 7 in the far-field region will be dominated by a linear combination of the three Hankel functions involving poles 5, 7, and 8 of Table I(A). As is well known, an asymptotic analysis of the Sommerfeld integral (3) for large ρ shows that the far-field expression of K_{xx}^A can be expressed as a linear combination of Hankel functions involving the poles of the exact spectral-domain Green's function $\widetilde{K}_{xx}^A$ on the real axis of the proper sheet of the complex k_ρ-plane, and each of these Hankel functions is weighted by the residue of $\widetilde{K}_{xx}^A$ at the corresponding pole (this linear combination of Hankel functions is, for instance, the term T_3 of [9, eqs. (3) and (4)]). The values of these poles and residues have been computed for the particular spectral-domain Green's function of Fig. 6 by means of an appropriate numerical algorithm [44], and the results are shown in Table I(B). The comparison of Table I(A) and (B) points out

that the real part of poles 5, 7, and 8 of Table I(A) coincide with those of the poles of Table I(B) within six significant figures. The real part of the residues at the aforementioned poles also coincide within four significant figures. Since the imaginary parts of all these poles and residues are negligible, the expression of K_{xx}^A inferred from (13) for large ρ matches with high accuracy the equivalent asymptotic closed-form expression arising from the Sommerfeld integral of (3). This coincidence in the approximate and exact asymptotic expressions justifies that the results obtained for the spatial-domain Green's functions in Figs. 4 and 7 are not only accurate for small ρ, but also for large ρ. Coming back to the discussion on the poles and residues 5, 7, and 8 of Table I(A) and those of Table I(B), it should be pointed out that the imaginary part of all these poles and residues should be zero. However, it is not zero owing to the finite precision of the numerical algorithms employed [34]. For practical purposes, this imaginary part is negligible and has been set to zero in the determination of the values of K_{xx}^A of Fig. 7 by means of (13). Please note that the imaginary part of pole 5 of Table I(A) is positive, which seems to contradict the criterion proposed for the choice of the poles used in (13) and (14). Again, this situation is a consequence of the finite precision of the method of total least squares, and it may occur when we apply the method to a lossless medium (such as that shown in Fig. 2) and one complex root $p_{n,i}^2$ of the polynomial $\widetilde{Q}_n^{(M)}(k_\rho^2)$ has a very small imaginary part (i.e., when $\mathrm{Im}\{p_{n,i}^2\} \lll \mathrm{Re}\{p_{n,i}^2\}$). In such a case, the sign of the pole $p_{n,i}$ to be used in (13) and (14) must be chosen so that $\mathrm{Re}\{p_{n,i}\} > 0$ since this pole tries to match a real pole of the original spectral-domain Green's function, and the corresponding Hankel function represents a traveling cylindrical wave with positive phase velocity (a consequence of this choice is that $\mathrm{Im}\{p_{n,i}\}$ may be positive as it happens with pole 5 of Table I). In this paper, we have only used this modified criterion for the choice of the sign of $p_{n,i}$ when $|\mathrm{Im}\{p_{n,i}\}/\mathrm{Re}\{p_{n,i}\}| < 10^{-5}$ and the medium is lossless. Numerical simulations have shown that, in the case of practical
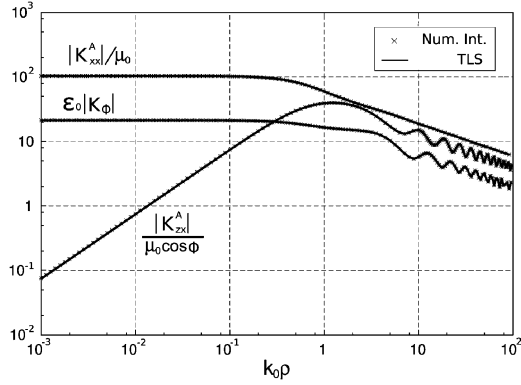
Fig. 12. Magnitude of spatial-domain Green's functions for the four-layer substrate microstrip structure shown in [24, Fig. 1]. Numerical integration results ($\times$) are compared with those obtained via (13) when $c_{0,M-1} = 0$ and via (14) when $c_{1,M-1} = c_{1,M-2} = 0$ (solid lines). $f = 11$ GHz, $z' = 0.4$ mm, $z = 1.4$ mm, $A = 0.1$, $T_0 = 3.7$, $M = 13$, $N = 29$.

lossy media, the standard criterion for the choice of the sign of $p_{n,i}$ applies, and all the poles used in (13) and (14) turn out to have a negative imaginary part. In the lossy case, the poles that control the far-field behavior of the spatial-domain Green's functions [i.e., the poles that play the role of 5, 7, and 8 in Table I(A)] also match with great accuracy the corresponding poles of the exact spectral-domain Green's functions [i.e., the poles that play the role of the poles in Table I(B)] both in the real and imaginary parts.

In Fig. 9, results are presented for the zx component of the spectral-domain vector-potential Green's function along the path of Fig. 1. The exact values of $\widetilde{K}_{zx}^A$ are compared with the values provided by (24), and excellent agreement is found once again. In this case, the spectral-domain Green's function $\widetilde{K}_{zx}^A$ has two TM poles and one TE pole on the real axis of the complex k_ρ-plane [7]. Fig. 10 shows the spatial counterpart of the spectral-domain Green's function plotted in Fig. 9. Specifically, Fig. 10 shows the results of K_{zx}^A obtained from (14) when the Hankel functions singularities are removed, and also when these singularities are not removed. The two sets of results are compared with results obtained via numerical integration of Sommerfeld integrals. As happens with the Green's functions plotted in Figs. 7 and 8, the Green's function K_{zx}^A plotted in Fig. 10 is not singular as $\rho \to 0$. Owing to this, the results shown in Fig. 10 when $c_{1,M-1} = c_{1,M-2} = 0$ (i.e., when the singularities are removed) are very accurate along eight decades of the variable $k_0\rho$, whereas the results obtained when $c_{1,M-1} \neq 0$ and $c_{1,M-2} \neq 0$ (the singularities are not removed) are incorrect for $k_0\rho < 10^{-1}$. The comparison of Figs. 8 and 10 shows that the error found in the approximation of K_{zx}^A when the singularities are not removed is much larger than that found in the approximation of K_{xx}^A. This fact can be attributed to the ρ^{-1}-type singularity of the Hankel functions $H_1^{(2)}(p_{1,i}\rho)$, which is much stronger than the logarithmic singularity of the Hankel functions $H_0^{(2)}(p_{0,i}\rho)$. In Fig. 11, we show another plot of K_{zx}^A in the particular case where this Green's function component is singular as $\rho \to 0$ (which occurs when the source and field points are placed at the air-dielectric interface of Fig. 2 as pointed out in [21] and [22]). Note that

the values of K_{zx}^A obtained via (14) match those obtained by means of numerical integration both for low ρ and for large ρ. In fact, the singularity of the type ρ^{-1} as $\rho \to 0$ [21] is very well reproduced by the function $G_1^{\text{ras}}(\rho)$ of (14).

Finally, Fig. 12 shows results for the spatial-domain Green's functions of the four-layer microstrip structure analyzed in [24, Fig. 1]. The source point is in the second layer and the field point is in the fourth layer. The Green's functions of Fig. 12 are also plotted in [24, Fig. 3]. It can be checked that excellent agreement exists between the results of [24], the results obtained by means of the closed-form expressions of (13) and (14), and the results obtained via numerical integration of Sommerfeld integrals. This clearly demonstrates that the technique presented here is also valid and very accurate for the computation of the Green's functions of arbitrary multilayered media.

IV. CONCLUSIONS

A new systematic technique has been introduced for the determination of closed-form expressions of the spatial-domain Green's functions for the scalar and vector potentials associated with the application of the mixed-potential integral equation in multilayered media. In the new technique, the Green's functions are fitted by means of a near-field term plus a finite sum of Hankel functions. The fitting coefficients are obtained by applying the method of total least squares. In the fitting process, special care is taken to remove the singularities of the Hankel functions as the horizontal separation between source and field points goes to zero. The results obtained with the new technique have been compared with numerical integration results. Excellent agreement has been found between the two sets of results both in the near- and the far-field regions. The removal of Hankel functions singularities has proven to be crucial for obtaining accurate results for the near field. Concerning the far field, the leading terms of the closed-form expressions have been found to match those obtained via analytic asymptotic techniques. A key point of the current technique is that it provides accurate results for a very wide range of distances with a computational expense that may be considerably smaller than that required by related previous techniques.

APPENDIX

The expressions of the spectral Green's functions $\widetilde{K}_\phi$, as well as the elements of the spectral dyadic Green's function $\overline{\overline{\mathbf{K}}}_A$ for the one-layer substrate microstrip structure of Fig. 2 are presented here. Also included are the asymptotic expressions of the spectral Green's functions that have been employed in (18) and (24) for obtaining the numerical results of Section III.

The spectral scalar potential Green's function $\widetilde{K}_\phi$ is given by the following:

$$
\begin{aligned}
\widetilde{K}_\phi(&k_\rho; z > 0 | z' > 0) \\
&= \frac{1}{2\epsilon_0 \tilde{u}_0} e^{-\tilde{u}_0 |z - z'|} \\
&\quad + \frac{(\epsilon_r \tilde{u}_0 + \tilde{u}_r \tanh \tilde{u}_r h)(\tilde{u}_0 - \tilde{u}_r \coth \tilde{u}_r h) - 2\tilde{u}_0^2(\epsilon_r - 1)}{2\epsilon_0 \tilde{u}_0 (\epsilon_r \tilde{u}_0 + \tilde{u}_r \tanh \tilde{u}_r h)(\tilde{u}_0 + \tilde{u}_r \coth \tilde{u}_r h)} \\
&\quad \times e^{-\tilde{u}_0(z + z')}
\end{aligned}
\tag{26}
$$

$$\widetilde{K}_\phi(k_\rho; -h < z < 0 | z' > 0)$$
$$= \frac{(\tilde{u}_0 + \tilde{u}_r \tanh \tilde{u}_r h) \, e^{-\tilde{u}_0 z'}}{\epsilon_0 \left(\epsilon_r \tilde{u}_0 + \tilde{u}_r \tanh \tilde{u}_r h\right)\left(\tilde{u}_0 + \tilde{u}_r \coth \tilde{u}_r h\right)}$$
$$\times \frac{\sinh \tilde{u}_r(z+h)}{\sinh \tilde{u}_r h} \tag{27}$$

where $\tilde{u}_0 = \sqrt{k_\rho^2 - k_0^2}$ and $\tilde{u}_r = \sqrt{k_\rho^2 - k_0^2 \epsilon_r}$. The asymptotic expressions of $\widetilde{K}_\phi$ can then be written as

$$\widetilde{K}_\phi^{\mathrm{as}}(k_\rho; z > 0 | z' > 0)$$
$$= \frac{1}{2\epsilon_0 k_\rho} \left(1 - e^{-k_\rho b}\right) e^{-k_\rho|z-z'|}$$
$$- \frac{(\epsilon_r - 1)}{2\epsilon_0 k_\rho(\epsilon_r + 1)} \left(1 - e^{-k_\rho b}\right) e^{-k_\rho(z+z')} \tag{28}$$

$$\widetilde{K}_\phi^{\mathrm{as}}(k_\rho; -h < z < 0 | z' > 0)$$
$$= \frac{1}{\epsilon_0(\epsilon_r + 1)k_\rho} \left(1 - e^{-k_\rho b}\right) e^{-k_\rho(z'-z)} \tag{29}$$

where $b = 1/(k_0 \sqrt{\epsilon_r})$ (in an arbitrary multilayered medium b should be taken as $b = 1/k_{\max}$, with $k_{\max}$ being the maximum wavenumber among the layers of the medium [38]). Note that the factor $\left(1 - e^{-k_\rho b}\right)$ has been deliberately introduced in (28) and (29) in order to avoid the singularity of the function $\widetilde{K}_\phi^{\mathrm{as}}$ when $k_\rho = 0$ [38]. Since the function $\widetilde{K}_\phi$ is not singular when $k_\rho = 0$, the function $\widetilde{K}_\phi^{\mathrm{as}}$ should not be singular either [remember that $\widetilde{K}_\phi^{\mathrm{as}}$ is involved in the approximation of $\widetilde{K}_\phi$, as shown in (6)].

The diagonal elements of $\overline{\overline{\mathbf{K}}}_A$ are $\widetilde{K}_{xx}^A$ and $\widetilde{K}_{zz}^A$ [37]. The expressions of $\widetilde{K}_{xx}^A = \widetilde{G}_{xx}^A$ can be written as

$$\widetilde{K}_{xx}^A(k_\rho; z > 0 | z' > 0)$$
$$= \frac{\mu_0}{2\tilde{u}_0} e^{-\tilde{u}_0|z-z'|} + \frac{\mu_0 \left(\tilde{u}_0 - \tilde{u}_r \coth \tilde{u}_r h\right)}{2\tilde{u}_0 \left(\tilde{u}_0 + \tilde{u}_r \coth \tilde{u}_r h\right)} e^{-\tilde{u}_0(z+z')} \tag{30}$$

$$\widetilde{K}_{xx}^A(k_\rho; -h < z < 0 | z' > 0)$$
$$= \frac{\mu_0 e^{-\tilde{u}_0 z'}}{(\tilde{u}_0 + \tilde{u}_r \coth \tilde{u}_r h)} \frac{\sinh \tilde{u}_r(z+h)}{\sinh \tilde{u}_r h} \tag{31}$$

and the asymptotic expressions of $\widetilde{K}_{xx}^A$ are given by

$$\widetilde{K}_{xx}^{A,\mathrm{as}}(k_\rho; z > 0 | z' > 0)$$
$$= \frac{\mu_0}{2k_\rho} \left(1 - e^{-k_\rho b}\right) e^{-k_\rho|z-z'|} \tag{32}$$

$$\widetilde{K}_{xx}^{A,\mathrm{as}}(k_\rho; -h < z < 0 | z' > 0)$$
$$= \frac{\mu_0}{2k_\rho} \left(1 - e^{-k_\rho b}\right) e^{-k_\rho(z'-z)}. \tag{33}$$

The expressions of $\widetilde{K}_{zz}^A = \widetilde{G}_{zz}^A + (\partial \tilde{P}_z / \partial z)$ are

$$\widetilde{K}_{zz}^A(k_\rho; z > 0 | z' > 0)$$
$$= \frac{\mu_0}{2\tilde{u}_0} e^{-\tilde{u}_0|z-z'|}$$
$$+ \frac{\mu_0 \left[(\epsilon_r \tilde{u}_0 - \tilde{u}_r \tanh \tilde{u}_r h)(\tilde{u}_0 + \tilde{u}_r \coth \tilde{u}_r h) + 2\tilde{u}_0^2(\epsilon_r - 1)\right]}{2\tilde{u}_0(\epsilon_r \tilde{u}_0 + \tilde{u}_r \tanh \tilde{u}_r h)(\tilde{u}_0 + \tilde{u}_r \coth \tilde{u}_r h)}$$
$$\times e^{-\tilde{u}_0(z+z')} \tag{34}$$

$$\widetilde{K}_{zz}^A(k_\rho; -h < z < 0 | z' > 0)$$
$$= \frac{\mu_0 \left(\epsilon_r \tilde{u}_0 + \tilde{u}_r \coth \tilde{u}_r h\right) e^{-\tilde{u}_0 z'}}{(\epsilon_r \tilde{u}_0 + \tilde{u}_r \tanh \tilde{u}_r h)(\tilde{u}_0 + \tilde{u}_r \coth \tilde{u}_r h)} \frac{\cosh \tilde{u}_r(z+h)}{\cosh \tilde{u}_r h} \tag{35}$$

and the asymptotic expressions of $\widetilde{K}_{zz}^A$ are

$$\widetilde{K}_{zz}^{A,\mathrm{as}}(k_\rho; z > 0 | z' > 0)$$
$$= \frac{\mu_0}{2k_\rho} \left(1 - e^{-k_\rho b}\right) e^{-k_\rho|z-z'|}$$
$$+ \frac{\mu_0(\epsilon_r - 1)}{k_\rho(\epsilon_r + 1)} \left(1 - e^{-k_\rho b}\right) e^{-k_\rho(z+z')} \tag{36}$$

$$\widetilde{K}_{zz}^{A,\mathrm{as}}(k_\rho; -h < z < 0 | z' > 0)$$
$$= \frac{\mu_0}{2k_\rho} \left(1 - e^{-k_\rho b}\right) e^{-k_\rho(z'-z)}. \tag{37}$$

The off-diagonal elements of $\overline{\overline{\mathbf{K}}}_A$ are $\widetilde{K}_{zx}^A$, $\widetilde{K}_{zy}^A$, $\widetilde{K}_{xz}^A$, and $\widetilde{K}_{yz}^A$ [37]. The expressions of $\widetilde{K}_{zx}^A = \widetilde{G}_{zx}^A$ and $\widetilde{K}_{zy}^A = \widetilde{G}_{zy}^A$ are

$$\frac{\widetilde{K}_{zx}^A}{jk_x}(k_\rho; z > 0 | z' > 0)$$
$$= \frac{\widetilde{K}_{zy}^A}{jk_y}(k_\rho; z > 0 | z' > 0)$$
$$= -\frac{\mu_0(\epsilon_r - 1)e^{-\tilde{u}_0(z+z')}}{(\epsilon_r \tilde{u}_0 + \tilde{u}_r \tanh \tilde{u}_r h)(\tilde{u}_0 + \tilde{u}_r \coth \tilde{u}_r h)} \tag{38}$$

$$\frac{\widetilde{K}_{zx}^A}{jk_x}(k_\rho; -h < z < 0 | z' > 0)$$
$$= \frac{\widetilde{K}_{zy}^A}{jk_y}(k_\rho; -h < z < 0 | z' > 0)$$
$$= -\frac{\mu_0(\epsilon_r - 1)e^{-\tilde{u}_0 z'}}{(\epsilon_r \tilde{u}_0 + \tilde{u}_r \tanh \tilde{u}_r h)(\tilde{u}_0 + \tilde{u}_r \coth \tilde{u}_r h)}$$
$$\times \frac{\cosh \tilde{u}_r(z+h)}{\cosh \tilde{u}_r h} \tag{39}$$

where k_x and k_y are the Cartesian spectral variables associated with x and y, respectively (and related to k_ρ via $k_\rho = \sqrt{k_x^2 + k_y^2}$). The asymptotic expressions of $\widetilde{K}_{zx}^A$ and $\widetilde{K}_{zy}^A$ are

$$\frac{\widetilde{K}_{zx}^{A,\mathrm{as}}}{jk_x}(k_\rho; z > 0 | z' > 0)$$
$$= \frac{\widetilde{K}_{zy}^{A,\mathrm{as}}}{jk_y}(k_\rho; z > 0 | z' > 0)$$
$$= -\frac{\mu_0(\epsilon_r - 1)}{2k_\rho^2(\epsilon_r + 1)} \left(1 - e^{-k_\rho b}\right)^2 e^{-k_\rho(z+z')} \tag{40}$$

$$\frac{\widetilde{K}_{zx}^{A,\mathrm{as}}}{jk_x}(k_\rho; -h < z < 0 | z' > 0)$$
$$= \frac{\widetilde{K}_{zy}^{A,\mathrm{as}}}{jk_y}(k_\rho; -h < z < 0 | z' > 0)$$
$$= -\frac{\mu_0(\epsilon_r - 1)}{2k_\rho^2(\epsilon_r + 1)} \left(1 - e^{-k_\rho b}\right)^2 e^{-k_\rho(z'-z)}. \tag{41}$$

Once again, the factor $\left(1 - e^{-k_\rho b}\right)^2$ has been introduced in (40) and (41) to avoid that $\widetilde{K}_{zx}^{A,\mathrm{as}}$ and $\widetilde{K}_{zy}^{A,\mathrm{as}}$ are singular when $k_\rho = 0$ [38]. Finally, $\widetilde{K}_{xz}^A = -jk_x\widetilde{P}_z$ and $\widetilde{K}_{yz}^A = -jk_y\widetilde{P}_z$ are related to $\widetilde{K}_{zx}^A$ and $\widetilde{K}_{zy}^A$ by means of

$$
\frac{\widetilde{K}_{xz}^A}{jk_x}(k_\rho; z > 0 | z' > 0)
$$
$$
= \frac{\widetilde{K}_{yz}^A}{jk_y}(k_\rho; z > 0 | z' > 0)
$$
$$
= -\frac{\widetilde{K}_{zx}^A}{jk_x}(k_\rho; z > 0 | z' > 0) \tag{42}
$$

$$
\frac{\widetilde{K}_{xz}^A}{jk_x}(k_\rho; -h < z < 0 | z' > 0)
$$
$$
= \frac{\widetilde{K}_{yz}^A}{jk_y}(k_\rho; -h < z < 0 | z' > 0)
$$
$$
= -\frac{\widetilde{K}_{zx}^A}{jk_x}(k_\rho; -h < z < 0 | z' > 0)\frac{\tanh \tilde{u}_r(z+h)}{\tanh \tilde{u}_r h} \tag{43}
$$

and, as a consequence of these relations, $\widetilde{K}_{xz}^{A,\mathrm{as}} = -\widetilde{K}_{zx}^{A,\mathrm{as}}$ and $\widetilde{K}_{yz}^{A,\mathrm{as}} = -\widetilde{K}_{zy}^{A,\mathrm{as}}$.

Looking at (28), (29), (32), (33), (36), and (37), it can be observed that the functions denoted in this paper by $\widetilde{G}_0^{\mathrm{as}}(k_\rho)$ (i.e., $\widetilde{K}_\phi^{\mathrm{as}}$, $\widetilde{K}_{xx}^{A,\mathrm{as}}$ and $\widetilde{K}_{zz}^{A,\mathrm{as}}$) are all linear combinations of functions of the type

$$
\tilde{f}_0(k_\rho) = \frac{\left(1 - e^{-k_\rho b}\right)}{k_\rho}e^{-k_\rho\Delta} \tag{44}
$$

where $\Delta \geq 0$. It means that the functions $G_0^{\mathrm{as}}(\rho)$ of (13) will all be linear combinations of functions of the type [42]

$$
f_0(\rho) = S_0\{\tilde{f}_0(k_\rho)\}
$$
$$
= \frac{1}{2\pi}\int_0^\infty J_0(k_\rho\rho)\left(1 - e^{-k_\rho b}\right)e^{-k_\rho\Delta}dk_\rho
$$
$$
= \frac{1}{2\pi}\left[\frac{1}{\sqrt{\rho^2 + \Delta^2}} - \frac{1}{\sqrt{\rho^2 + (b+\Delta)^2}}\right]. \tag{45}
$$

If $\Delta = 0$, the functions $f_0(\rho)$ show a singularity of the type ρ^{-1} as $\rho \to 0$. In accordance with (28), (29), (32), (33), (36), and (37), this means that, in the case $z = z'$, the functions $G_0^{\mathrm{as}}(\rho)$ will show the same singularity as $\rho \to 0$. According to (3) and (13), the singularity will also be present in $G_0(\rho)$, which is in agreement with the near-field behavior of $G_0(\rho)$ described in [20].

According to (40) and (41), the functions denoted in this paper by $\widetilde{G}_1^{\mathrm{as}}(k_\rho)$ (i.e., $\widetilde{K}_{zx}^{A,\mathrm{as}} = -\widetilde{K}_{xz}^{A,\mathrm{as}}$ and $\widetilde{K}_{zy}^{A,\mathrm{as}} = -\widetilde{K}_{yz}^{A,\mathrm{as}}$) are functions of the type

$$
\tilde{f}_1(k_\rho) = \frac{\left(1 - e^{-k_\rho b}\right)^2}{k_\rho^2}e^{-k_\rho\Delta} \tag{46}
$$

where $\Delta \geq 0$. Therefore, the functions $G_1^{\mathrm{as}}(\rho)$ of (14) will be

functions of the type [42]

$$
f_1(\rho) = S_1\{\tilde{f}_1(k_\rho)\}
$$
$$
= \frac{1}{2\pi}\int_0^\infty J_1(k_\rho\rho)\left(1 - e^{-k_\rho b}\right)^2 e^{-k_\rho\Delta}dk_\rho
$$
$$
= \frac{1}{2\pi\rho}\left[\frac{2(b+\Delta)}{\sqrt{\rho^2 + (b+\Delta)^2}} - \frac{\Delta}{\sqrt{\rho^2 + \Delta^2}}\right.
$$
$$
\left. - \frac{2b+\Delta}{\sqrt{\rho^2 + (2b+\Delta)^2}}\right]. \tag{47}
$$

It can be shown that $f_1(\rho) \propto \rho$ as $\rho \to 0$ and $\Delta \neq 0$, but $f_1(\rho) \propto \rho^{-1}$ as $\rho \to 0$ and $\Delta = 0$. Looking at (40) and (41), this means that in the case $z = z' = 0$ (i.e., the source and field and points are placed at the interface between the air and the dielectric layer in Fig. 2), the functions $G_1^{\mathrm{as}}(\rho)$ will show a singularity of the type ρ^{-1} as $\rho \to 0$. According to (4) and (14), this singularity will be reproduced in $G_1(\rho)$, which is in agreement with the behavior of $G_1(\rho)$ predicted in [21].

REFERENCES

[1] J. R. Mosig, "Arbitrarily shaped microstrip structures and their analysis with a mixed-potential integral equation," *IEEE Trans. Microw. Theory Tech.*, vol. 36, no. 2, pp. 314–323, Feb. 1988.

[2] R. C. Hall and J. R. Mosig, "The analysis of arbitrarily shaped aperture-coupled patch antennas via a mixed-potential integral equation," *IEEE Trans. Antennas Propag.*, vol. 44, no. 5, pp. 608–614, May 1996.

[3] K. A. Michalski and D. Zheng, "Electromagnetic scattering and radiation by surfaces of arbitrary shape in layered media—Part II: Implementation and results for contiguous half-spaces," *IEEE Trans. Antennas Propag.*, vol. 38, no. 3, pp. 345–352, Mar. 1990.

[4] S. Vitebskiy, K. Sturgess, and L. Carin, "Short-pulse plane-wave scattering from buried perfectly conducting bodies of revolution," *IEEE Trans. Antennas Propag.*, vol. 44, no. 2, pp. 143–151, Feb. 1996.

[5] J. R. Mosig, "Integral equation technique," in *Numerical Techniques for Microwave and Millimeter-Wave Passive Structures*, T. Itoh, Ed. New York: Wiley, 1989, pp. 133–213.

[6] K. A. Michalski and J. R. Mosig, "Multilayered media Green's functions in integral equation formulations," *IEEE Trans. Antennas Propag.*, vol. 45, no. 3, pp. 508–519, Mar. 1997.

[7] J. R. Mosig and F. E. Gardiol, "Analytical and numerical techniques in the Green's function treatment of microstrip antennas and scatterers," *Proc. Inst. Elect. Eng.*, vol. 130, no. 2, pt. H, pp. 175–182, Mar. 1983.

[8] K. A. Michalski, "Extrapolation methods for Sommerfeld integral tails," *IEEE Trans. Antennas Propag.*, vol. 46, no. 10, pp. 1405–1418, Oct. 1998.

[9] J. R. Mosig and Álvarez-Melcón, "Green's functions in lossy layered media: Integration along the imaginary axis and asymptotic behavior," *IEEE Trans. Antennas Propag.*, vol. 51, no. 12, pp. 3200–3208, Dec. 2003.

[10] T. J. Cui and W. C. Chew, "Fast evaluation of Sommerfeld integrals for EM scattering and radiation by three-dimensional buried objects," *IEEE Trans. Geosci. Remote Sens.*, vol. 37, no. 3, pp. 887–900, Mar. 1999.

[11] W. Cai and T. Yu, "Fast calculations of dyadic Green's functions for electromagnetic scattering in a multilayer medium," *J. Comput. Phys.*, vol. 165, pp. 1–21, 2000.

[12] L. Tsang, C. J. Ong, C. C. Huang, and V. Jandhyala, "Evaluation of the Green's function for the mixed potential integral equation (MPIE) method in the time domain for layered media," *IEEE Trans. Antennas Propag.*, vol. 51, no. 7, pp. 1559–1571, Jul. 2003.

[13] S. Barkeshli, P. H. Pathak, and M. Marin, "An asymptotic closed-form microstrip surface Green's function for the efficient moment method analysis of mutual coupling in microstrip antennas," *IEEE Trans. Antennas Propag.*, vol. 38, no. 9, pp. 1374–1383, Sep. 1990.

[14] Y. Brand, A. Álvarez-Melcón, J. R. Mosig, and R. C. Hall, "Large distance behavior of stratified media spatial Green's functions," in *IEEE AP-S Int. Symp. Dig.*, Montreal, QC, Canada, Jul. 1997, pp. 2334–2337.

[15] D. G. Fang, J. J. Yang, and G. Y. Delisle, "Discrete image theory for horizontal electric dipoles in a multilayered medium," *Proc. Inst. Elect. Eng.*, vol. 135, no. 5, pt. H, pp. 297–303, Oct. 1988.

[16] Y. L. Chow, J. J. Yang, D. G. Fang, and G. E. Howard, "A closed-form spatial Green's function for the thick microstrip substrate," *IEEE Trans. Microw. Theory Tech.*, vol. 39, no. 3, pp. 588–592, Mar. 1991.

[17] R. A. Kipp and C. H. Chan, "Complex image method for sources in bounded regions of multilayer structures," *IEEE Trans. Microw. Theory Tech.*, vol. 42, no. 5, pp. 860–865, May 1994.

[18] M. I. Aksun, "A robust approach for the derivation of closed-form Green's functions," *IEEE Trans. Microw. Theory Tech.*, vol. 44, no. 5, pp. 651–658, May 1996.

[19] N. Kinayman and M. I. Aksun, "Efficient use of closed-form Green's functions for the analysis of planar geometries with vertical connections," *IEEE Trans. Microw. Theory Tech.*, vol. 45, no. 5, pp. 593–603, May 1997.

[20] C. H. Chan and R. A. Kipp, "Application of the complex image method to multilevel, multiconductor microstrip lines," *Int. J. Microw. Millimeter-Wave Comput.-Aided Eng.*, vol. 7, no. 5, pp. 359–367, 1997.

[21] ——, "Application of the complex image method to characterization of microstrip vias," *Int. J. Microw. Millimeter-Wave Comput.-Aided Eng.*, vol. 7, no. 5, pp. 368–379, 1997.

[22] N. Hojjat, S. Safavi-Naeini, R. Faraji-Dana, and Y. L. Chow, "Fast computation of the nonsymmetrical components of the Green's function for multilayer media using complex images," *Proc. Inst. Elect. Eng.—Microw. Antennas Propag.*, vol. 145, no. 4, pp. 285–288, Aug. 1998.

[23] N. Hojjat, S. Safavi-Naeini, and Y. L. Chow, "Numerical computation of complex image Green's functions for multilayer dielectric media: Near-field zone and the interface region," *Proc. Inst. Elect. Eng.–Microw. Antennas Propag.*, vol. 145, no. 6, pp. 449–454, Dec. 1998.

[24] F. Ling and J. M. Jin, "Discrete complex image method for Green's functions of general multilayer media," *IEEE Microw. Guided Wave Lett.*, vol. 10, no. 10, pp. 400–402, Oct. 2000.

[25] Y. Liu, L. W. Li, T. S. Yeo, and M. S. Leong, "Application of DCIM to MPIE–MoM analysis of 3-D PEC objects in multilayered media," *IEEE Trans. Antennas Propag.*, vol. 50, no. 2, pp. 157–162, Feb. 2002.

[26] Y. Ge and K. P. Esselle, "New closed-form Green's functions for microstrip structures-theory and results," *IEEE Trans. Microw. Theory Tech.*, vol. 50, no. 6, pp. 1556–1560, Jun. 2002.

[27] N. V. Shuley, R. R. Boix, F. Medina, and M. Horno, "On the fast approximation of Green's functions in MPIE formulations for planar-layered media," *IEEE Trans. Microw. Theory Tech.*, vol. 50, no. 9, pp. 2185–2192, Sep. 2002.

[28] P. Yla-Oijala and M. Taskinen, "Efficient formulation of closed-form Green's functions for general electric and magnetic sources in multilayered media," *IEEE Trans. Antennas Propag.*, vol. 51, no. 8, pp. 2106–2115, Aug. 2003.

[29] S. A. Teo, S. T. Chew, and M. S. Leong, "Error analysis of the discrete complex image method and pole extraction," *IEEE Trans. Microw. Theory Tech.*, vol. 51, no. 2, pp. 406–413, Feb. 2003.

[30] M. I. Aksun and G. Dural, "Clarification of issues on the closed-form Green's functions in stratified media," *IEEE Trans. Antennas Propag.*, vol. 53, no. 11, pp. 3644–3653, Nov. 2005.

[31] M. Yuan, T. K. Sarkar, and M. Salazar-Palma, "A direct discrete complex image method from the closed-form Green's functions in multilayered media," *IEEE Trans. Microw. Theory Tech.*, vol. 54, no. 3, pp. 1025–1032, Mar. 2006.

[32] V. I. Okhmatovski and A. C. Cangellaris, "A new technique for the derivation of closed-form electromagnetic Green's functions for unbounded planar layered media," *IEEE Trans. Antennas Propag.*, vol. 50, no. 7, pp. 1005–1016, Jul. 2002.

[33] ——, "Evaluation of layered media Green's functions via rational function fitting," *IEEE Microw. Wireless Compon. Lett.*, vol. 14, no. 1, pp. 22–24, Jan. 2004.

[34] V. N. Kourkoulos and A. C. Cangellaris, "Accurate approximation of Green's functions in planar stratified media in terms of a finite sum of spherical and cylindrical waves," *IEEE Trans. Antennas Propag.*, vol. 54, no. 5, pp. 1568–1576, May 2006.

[35] E. Simsek, Q. H. Liu, and B. Wei, "Singularity subtraction for evaluation of Green's functions for multilayer media," *IEEE Trans. Microw. Theory Tech.*, vol. 54, no. 1, pp. 216–225, Jan. 2006.

[36] R. S. Adve, T. K. Sarkar, S. M. Rao, E. K. Miller, and D. R. Pflug, "Application of the Cauchy method for extrapolating/interpolating narrow-band system responses," *IEEE Trans. Microw. Theory Tech.*, vol. 45, no. 5, pp. 837–845, May 1997.

[37] K. A. Michalski and D. Zheng, "Electromagnetic scattering and radiation by surfaces of arbitrary shape in layered media—Part I: Theory," *IEEE Trans. Antennas Propag.*, vol. 38, no. 3, pp. 335–344, Mar. 1990.

[38] F. J. Demuynck, G. A. E. Vandenbosch, and A. R. Van de Capelle, "The expansion wave concept—Part I: Efficient calculation of spatial Green's functions in a stratified dielectric medium," *IEEE Trans. Antennas Propag.*, vol. 46, no. 3, pp. 397–406, Mar. 1998.

[39] B. Gustavsen and A. Semylen, "Rational approximation of frequency domain responses by vector fitting," *IEEE Trans. Power Del.*, vol. 14, no. 3, pp. 1052–1061, Jul. 1999.

[40] J. Rahman and T. K. Sarkar, "Deconvolution and total least squares in finding the impulse response of an electromagnetic system from measured data," *IEEE Trans. Microw. Theory Tech.*, vol. 54, no. 4, pp. 416–421, Apr. 1995.

[41] A. Edelman and H. Murakami, "Polynomial roots from companion matrix eigenvalues," *Math. Comput.*, vol. 64, no. 210, pp. 763–776, 1995.

[42] L. S. Gradshteyn and L. M. Ryzhik, *Table of Integrals, Series and Products*, 6th ed. San Diego, CA: Academic, 2000.

[43] M. Abramowitz and I. Stegun, *Handbook of Mathematical Functions*, 9th ed. New York: Dover, 1970.

[44] R. Rodríguez-Berral, F. Mesa, and F. Medina, "Systematic and efficient root finder for computing the modal spectrum of planar layered waveguides," *Int. J. Microw. Millimeter-Wave Comput.-Aided Eng.*, vol. 14, pp. 73–83, Jan. 2004.

Rafael R. Boix (M'96) received the Licenciado and Doctor degrees in physics from the University of Seville, Seville, Spain, in 1985 and 1990 respectively.

Since 1986, he has been with the Electronics and Electromagnetism Department, University of Seville, where, in 1994, he became an Associate Professor. His current research interests are focused on the numerical analysis of periodic electromagnetic structures with applications to the design of frequency-selective surfaces and electromagnetic bandgap passive circuits.

Francisco Mesa (M'93) was born in Cádiz, Spain, on April 1965. He received the Licenciado and Doctor degrees in physics from the University of Seville, Seville, Spain, in 1989 and 1991, respectively.

He is currently an Associate Professor with the Department of Applied Physics 1, University of Seville. His research interest is focused on electromagnetic propagation/radiation in planar lines with general anisotropic materials.

Francisco Medina (M'90–SM'01)was born in Puerto Real, Cádiz, Spain, in November 1960. He received the Licenciado and Doctor degrees in physics from the University of Seville, Seville, Spain, in 1983 and 1987 respectively.

From 1986 to 1987, he spent the academic year with the Laboratoire de Microondes de l'ENSEEIHT, Toulouse, France. From 1985 to 1989, he was an Assistant Professor with the Department of Electronics and Electromagnetism, University of Seville, where, since 1990, he has been an Associate Professor of electromagnetism. He is also currently Head of the Microwaves Group, Department of Electronics and Electromagnetism, University of Seville. He is on the Editorial Board of the *International Journal of RF and Microwave Computer-Aided Engineering*. He is also a reviewer for the Institution of Electrical Engineers (IEE), U.K., and American Physics Association journals. His research interest includes analytical and numerical methods for guiding, resonant, and radiating structures, passive planar circuits, periodic structures, and the influence of anisotropic materials (including microwave ferrites) on such systems. He is also interested in artificial media modeling and design.

Dr. Medina was a member of the Technical Programme Committees (TPC) of the 23rd European Microwave Conference, Madrid, Spain (1993), ISRAMT'99, Málaga, Spain (1999), and Microwaves Symposium'00, Tetouan, Morocco (2000). He was co-organizer of the "New Trends on Computational Electromagnetics for Open and Boxed Microwave Structures" Workshop, Madrid, Spain (1993). He is a member of the Massachusetts Institute of Technology (MIT) Electromagnetics Academy. He is on the review board of the IEEE TRANSACTIONS ON MICROWAVE THEORY AND TECHNIQUES. He also acts as a reviewer for other IEEE publications. He was the recipient of a 1983 research scholarship presented by the Spanish Ministerio de Educación y Ciencia (MEC). He was also the recipient of a scholarship presented by the French Ministère de la Recherche et la Technologie.